Available online at www.sciencedirect.com
ScienceDirect
Acta Materialia 56 (2008) 1257–1273
Acta MATERIALIA
www.elsevier.com/locate/actamat

A framework for automated analysis and simulation of 3D polycrystalline microstructures. Part 1: Statistical characterization

Michael Groeber [a,*], Somnath Ghosh [b], Michael D. Uchic [c], Dennis M. Dimiduk [c]

[a] *Materials Science and Engineering, The Ohio State University, Columbus, OH 43210, USA*
[b] *Mechanical Engineering and Materials Science and Engineering, The Ohio State University, Columbus, OH 43210, USA*
[c] *Air Force Research Laboratory, Materials and Manufacturing Directorate, AFRL/MLLMD, Wright-Patterson AFB, OH 45433, USA*

Received 7 April 2007; received in revised form 11 October 2007; accepted 15 November 2007
Available online 28 January 2008

Abstract

This is the first of a two-part paper aimed at developing a robust framework for the collection, quantification and simulation of 3D polycrystalline microstructures. Serial-sectioning methods are used to generate data that characterize the microstructural morphology and crystallography of grains. The microstructure simulation model and codes take as input a series of electron backscatter diffraction (EBSD) patterns from the serial-sectioning experiments. Robust statistical analysis of the grain-level microstructures in 3D is conducted in this part of this paper. This analysis can provide necessary information for modeling and simulation efforts in the form of a highly refined and unbiased description of specific features, such as the distribution of grain size, shape and orientation.
Published by Elsevier Ltd on behalf of Acta Materialia Inc.

Keywords: Serial-sectioning; Electron backscattering diffraction (EBSD); Crystal structure; Modeling

1. Motivation

This two-part paper develops a comprehensive method for the generation of virtual polycrystalline microstructures that can be used in computational modeling for prediction of microstructure–property relations. The importance of microstructure relative to material properties is a basic tenet of materials science and engineering. With the continued improvement in modern computing capabilities, the ability to include local microstructural features in simulations of microstructure evolution or materials performance is an active area of research [1–3]. However, there has been a general disconnect between the ability to characterize microstructure and efforts to represent this information in simulations. For example, most grain structures are known to have non-uniform distributions of size and shape, and can also exhibit large variations in morphology and crystallography [4]. This realization clearly identifies a shortcoming when grain morphology is represented by a uniform array of basic shapes like spheres, cubes, or simple polyhedra to fill space, as done in many simulation studies [5–7].

Rollett et al. [8,9] made significant improvements on the ability to generate virtual 3D microstructures. Their methodology is linked to real microstructures through the collection of statistical distributions of grain size and shape in 2D. Those distributions are used to infer the 3D structure, and then used to bound a synthetic microstructure generation process. One advantage of their methodology is that the experimental data can be collected in a straightforward manner with a relatively short time for data collection. Recently, Lewis and Geltmacher [10] have used image-based methods to create virtual grain ensembles. That effort has relied on the collection of serial-section data

* Corresponding author. Tel.: +1 614 203 1403.
E-mail addresses: groeber.9@osu.edu (M. Groeber), ghosh.5@osu.edu (S. Ghosh), Michael.Uchic@wpafb.af.mil (M.D. Uchic), Dennis.Dimiduk@wpafb.af.mil (D.M. Dimiduk).

1359-6454/$34.00 Published by Elsevier Ltd on behalf of Acta Materialia Inc.
doi:10.1016/j.actamat.2007.11.041

to reconstruct polycrystalline microstructures that are subsequently used within a finite element mesh and model. This technique is attractive in its ability to translate real microstructures into a computational form with few extrapolations or assumptions. While these studies are no doubt innovative, they have some limitations. The work in Refs. [8,9] considers only the distribution of size and shape of grains in creating the synthetic microstructures. Other morphological characteristics, such as the number of contiguous neighbors per grain and the correlations between different parameters, are sometimes are very important, but have not been incorporated in that work. Additionally, the size and shape measurements reported in Refs. [8,9] have been collected from 2D sections and then extrapolated to 3D. This allows for potential errors in representing the actual 3D distributions. The tessellation and grain assignment process in Refs. [8,9] may in some cases produce unrealistic or anomalous grain shapes. On the other hand, the work in Ref. [10] is for deterministic structures, having bypassed the need for statistical characterization and synthetic structure generation. The collection of the microstructural data for each microstructure model can be extremely time-consuming. Additionally, direct conversion of discrete voxel data in this method creates artificially aliased grain boundary topologies.

The goal of the present work is to create a comprehensive microstructure simulator from 3D experimental data that can feed into an effective computational model. Some aspects of the previous developments have been taken into consideration in the present framework. The first of this two-part paper will focus solely on the statistical characterization of grain-level microstructures in 3D from serial-section data, while the second part will discuss the application of these statistical descriptions to generate equivalent grain structures that are suitable for modeling and simulation.

2. Introduction and scope of Part 1

The ability to characterize microstructural features using statistical methods is an important advancement in materials science, because it can allow for more accurate predictions of material properties. Classical stereological methods involve prediction of 3D microstructural characteristics from image data analysis of a sectioned surface. However, there are a number of microstructural parameters that cannot be determined from a single 2D section, such as feature connectivity, true feature shape and the number of features per unit volume [11]. The need to characterize microstructures more completely has led to the development of methods that allow one to obtain 3D microstructural data of grain structures directly, such as serial-sectioning [12–15], intergranular corrosion [16] and various X-ray tomography based techniques [17,18].

Even though there have been advancements in 3D characterization methods [19–21], there have been few studies that have examined the extremities and local neighborhoods present in polycrystalline microstructures. Many individual parameters have been quantified in 2D and some in 3D, but much less frequently are the relationships between multiple parameters studied [19]. The focus of this paper is to quantify a suite of microstructural parameters as well as their correlations to define morphological characteristics.

Serial-sectioning via a dual beam focused ion beam-scanning electron microscope (DB FIB-SEM) outfitted with electron back-scatter diffraction (EBSD) capabilities is used to collect crystallographic data in 3D. The process of data collection is described in detail in Ref. [14] and the reconstruction and processing of the data is described in Refs. [22,23]. The subsequent statistical analysis to develop distribution and correlation functions is the focus of this paper.

3. FIB-EBSD serial-sectioning methodology and material details

3.1. Sectioning and data processing methodology

A brief outline of the serial-sectioning data collection and processing details are given here:

- The DB FIB-SEM is used to section the sample repeatedly with the ion beam and collect crystallographic orientation maps for each section using EBSD. An advantage of acquiring EBSD maps is that it allows for unsupervised segmentation of grains and grain boundaries, which can be difficult to perform using only image data.
- Rough alignment of the series of 2D EBSD maps is performed by a convolution process, as the maps may initially be slightly misaligned. The convolution technique involves matching intensity values of consecutive EBSD maps and generally ensures sections are within 1–2 pixels of their correct position. The series of EBSD maps are then combined to provide a 3D dataset that can be analyzed. During this alignment process (and the refined alignment process discussed later), only translations (x and y movements) are applied to the sections. As a result, the Euler angles associated with the data points should not be affected, and thus no rotation of these angles is necessary.
- Following initial alignment, grain identification and segmentation is performed. The misorientation of neighboring voxels is determined and used to group voxels together as grains [14,22,23]. Details of the definition and calculation procedure of misorientation are discussed in Ref. [24]. Misorientation is described in terms of a rotation axis vector n, which represents a common axis for both crystal lattices, and an angle θ, which is the rotation about n needed to bring the two crystal lattices into coincidence. The rotation angle is given by

$$\theta = \min \left| \cos^{-1} \left\{ \frac{\mathrm{tr}(g_B g_A^{-1} O) - 1}{2} \right\} \right| \quad (1)$$

where, g_A and g_B are the orientation matrices of grain A and B, respectively, and O is the crystal symmetry operator. For this work, voxels are grouped together and assigned to the same grain if the misorientation between their immediate neighboring voxels is below a user-defined critical value (5°). For the IN100 sample investigated in this work, there was little orientation spread within each grain. The orientation variation in-plane and between sections was; in general, only fractions of a degree with the majority of grains having a grain average misorientation (average of the misorientations between each voxel's orientation and the grain's average orientation) below 1°.

- Following grain identification, data cleaning routines are used to refine the quality of the data set. There are two filters that are applied to the data to remove extremely small and poor quality grains [22,23]. The poor quality filter is implemented to account for small pores and particles in the material. The minimum allowable grain size in this work is twenty-four (24) contiguous voxels, which for the voxel size in this dataset corresponds to a diameter of ~0.5 μm. Any set of voxels below the minimum size are broken apart and assigned to neighboring grains. During reassignment, each voxel is assigned to the grain with which it shares the most surface area. The quality filter calls on the measure of data quality assigned to each voxel by the EBSD collection program. If a grain contains no voxels above a minimum quality tolerance, then the grain is removed and the voxels are assigned to neighboring grains. Occasionally, pores and particles contained slightly more than 24 voxels, but none were of sufficient quality.
- After data clean-up, a more refined alignment procedure is used to reduce the misalignment between the individual 2D EBSD maps further [22,23]. During the second alignment, the misorientation between each voxel in an individual 2D section and the voxel directly above it in the previous section is computed. The section is then shifted in the x and y direction, checking the misorientations at each adjusted position. The position which results in the fewest orientation differences (defined as a voxel being misoriented by more than 5° from the corresponding voxel in the previous section) is chosen as the ideal position. Effectively hundreds of "disks" through the grains are aligned simultaneously, creating a high-fidelity alignment. The position with the fewest orientation differences is generally the position that places the most disks directly on top of the corresponding disk in the previous section.

Though each step of the data collection and processing is automated, the total time required for completing these procedures is not small. Collection of the sections commands the most time at approximately 3 days for a dataset of the size presented. The processing is less temporally intrusive, taking less than a day to complete. The first alignment procedure, grain segmentation and data clean-up, and second alignment procedure take approximately 1, 6 and 1 h, respectively, for a dataset of this size.

3.2. Material details

The data collection process is used to sample the microstructure of forged and sub-solvus heat-treated IN100, a nickel-base superalloy produced by powder-metallurgy processing. The volume obtained from reconstruction of the individual sections is shown in Fig. 1. The experimental volume, which measures 96 μm × 36 μm × 46 μm, samples 4373 grains including surface grains in total and 2704 full grains. An important note is that only grains contained fully inside the experimentally collected volume are considered during subsequent analysis. This measure is taken to remove the bias on the morphology of grains intersecting the edges of the volume. However, a bias against larger grains is possibly introduced, due to the increased probability of a large grain intersecting the volume's surface. A second method for excluding grains was implemented to remove morphological biases, while limiting any size bias. This method is exactly analogous to the 2D technique of creating a counting frame. The idea and practice of using counting frames is discussed by Gunderson [25]. The sets of grains obtained from the two methods were compared to quantify their differences. It was noted that the two sets appeared to be statistically similar for all of the parameters that will be presented in this paper. However, the second set of grains contained far fewer grains (1690) than the first set (2704). The similarity of the grain sets led to the conclusion that both sets likely contain enough grains to describe mean-field statistics and neither contains enough grains to describe extreme-value statistics. From this point forward, the analysis presented is of the first grain set, chosen mainly for the larger number of grains.

The microstructure of IN100, shown in Fig. 2 as an ion-induced secondary electron (ISE) image, presents advantages and complications for the FIB and EBSD experimental technique. A main advantage is the fine grain size (~3 μm average diameter), which allows for many grains to be contained in the meso-scale volume that can be interrogated by the DB FIB-SEM. In part, the grain size remains fine during the alloy processing because of a distribution of fine carbide particles which have been ignored in this study. A minor complication that arises is that the superalloy processing results in two microconstituents for each grain. Most of the volume (~80%) consists of a dual-phase microconstituent consisting of the γ-phase matrix containing fine γ′-phase coherent precipitates. The remaining ~20% of the volume consists of the primary γ′ microconstituent which appears as single-phase grains in Fig. 2. Actually, the primary γ′ microconstituent maintains a region of semi-coherent interface with its parent grain thus being nominally indistinguishable from that grain on the basis of crystallographic orientation via EBSD pattern analysis. Chemical

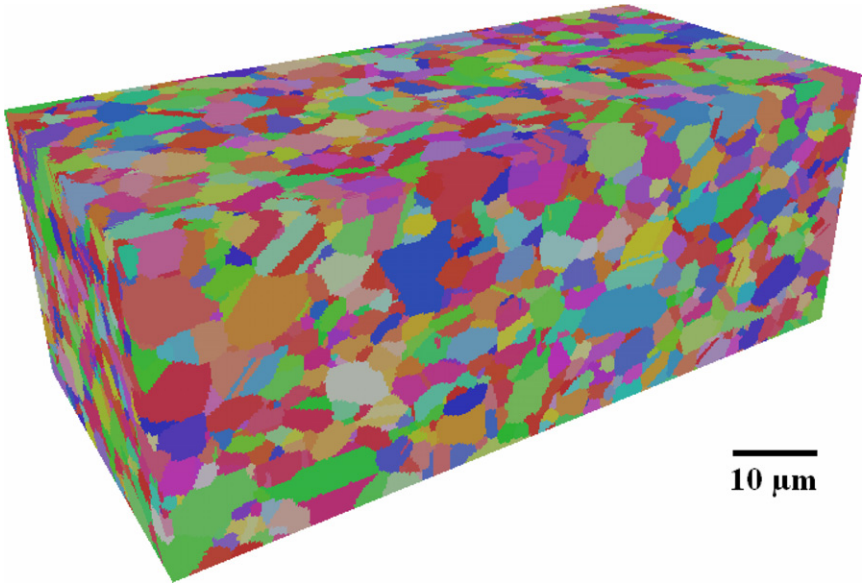

Fig. 1. 3D reconstruction of IN100 Ni-based superalloy. The volume shown is the reconstruction of individual EBSD maps collected during the serial-sectioning experiment and has dimensions 96 μm × 36 μm × 46 μm.

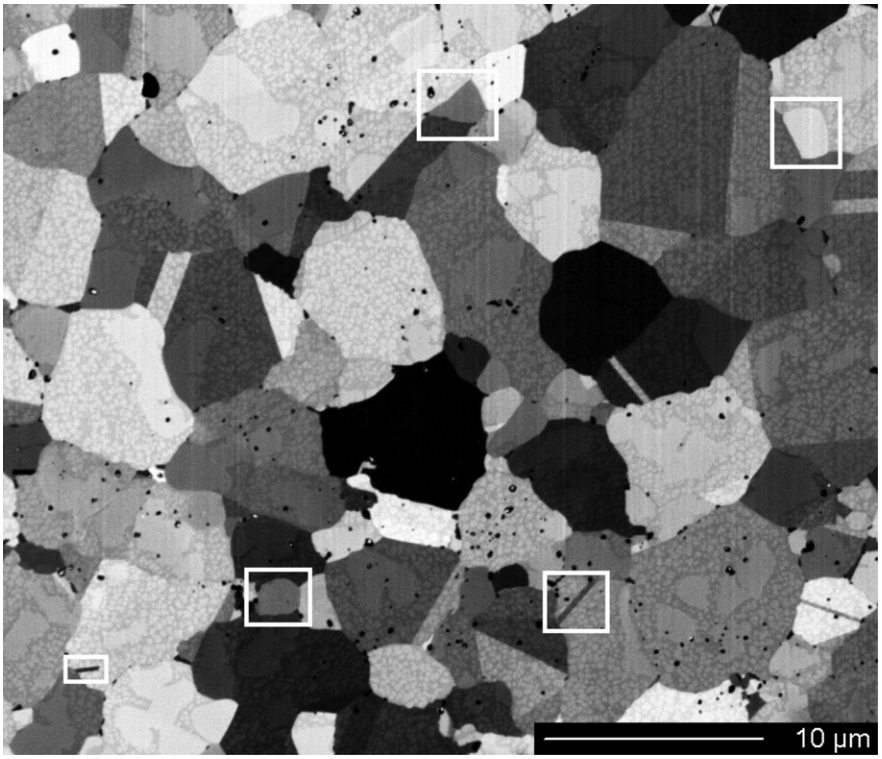

Fig. 2. Ion-induced secondary electron (ISE) image of IN100. The presence of two microconstituents and thin annealing twins presents a challenge during the segmentation and quantification of the microstructure. Several examples of these features are highlighted in the image.

mapping or backscatter electron imaging in conjunction with the EBSD maps could possibly alleviate this issue, but this data was not available with the microscope used in this work. Therefore, when performing the statistical analysis, the two-microconstituent microstructure is treated as having only one type of grains. The second complication with the experimental data is that the resolution is not sufficient to sample accurately many of the twins that are frequently observed in the microstructure. The twins tend to be thin (~0.25–0.5 μm) in one dimension and in many cases they are nearly the same size as the voxel size. To eliminate this problem, the twins are merged with their 'parent' grains. Effects of both of these issues will be considered further in the following paragraphs.

There are limitations with the current data-collection procedure which affect the ability to fully quantify the microstructure of this nickel-base superalloy. However, a number of these issues can be solved by simply increasing the resolution of the data collected and collecting more data; but, others require more substantial changes to the methods as discussed in the following.

The resolution of the data is extremely important in producing accurate statistics. A rule of thumb for 'quality' reconstructions and by association statistics is that a minimum of ~10 sections are needed through a feature. Some studies [26] have concluded that as many as 50–150 sections are needed to describe shape accurately. Applying this general rule to the current dataset shows the need for increased resolution. In this study, approximately 90% of all grains have at least 10 sections through their largest dimension. However, only ~53% of all grains also have at least 10 sections through their smallest dimension.

Much like the resolution of the data, the number of grains in the experimental volume is extremely important. A large enough number of grains are necessary to generate representative distributions. The 2704 grains used in this analysis are sufficient for the distributions of the individual parameters and most aspects of the correlation distributions. In general, each bin in the individual parameter distributions and correlation distributions contains hundreds of grains. However, the number of grains analyzed fell short for proper analysis of some aspects of the correlation distributions. First, for all correlations only diameter bins between 1 and 7 microns are considered, because the larger diameter bins are underpopulated. A minimum number of 50 grains in a diameter bin has been selected as the cutoff for consideration. Secondly, multiple correlations are not possible due to the limited number of grains. The number of grains necessary for a given relationship tended towards N^x, where N is the number of grains necessary for an individual distribution and x is the number of correlations. Using this relationship and the selected minimum of 50, ~125,000 grains would be needed for a correlation between three parameters.

The poor sampling of twins and their subsequent merging certainly affects the distributions of most parameters. The volume distribution shifts toward smaller volumes when twins are not removed as shown in Fig. 3. Additionally, the number of contiguous neighbors for most grains would likely increase with the reintroduction of twins. Fig. 2 also shows the effect on grain shape when twins are not merged. The twin grains tend to have a distinct shape, often more plate-like, which is present on the plot after reintroduction of twins.

Lastly, the EBSD software is not capable of distinguishing the two microconstituents in the material with the settings used in this experiment. Statistically this presents a problem because the two microconstituents have a clear difference in size when viewed using backscatter electron (BSE) images or ISE images, as seen in Fig. 2. The γ' microconstituent particles or grains are often significantly smaller than their neighboring dual-phase $\gamma + \gamma'$ grains. Thus, it is expected that the volume distribution of only the $\gamma + \gamma'$ grains would shift to larger volumes and become less strongly lognormal if the two microconstituents were segregated and plotted separately. The current dataset remains limited by this issue, but future experiments utilizing chemical mapping or backscatter electron imaging appear promising and should alleviate this problem.

4. Statistical analysis

The direct measurement of microstructural parameters in 3D allows one to describe features without the need for stereological interpolation and enables a higher fidelity characterization. Additionally, if each individual constituent of the polycrystalline microstructure e.g. grains is measured, it allows for the developments of distributions of parameters, rather than simply average values. This more detailed description can provide information about the higher order moments of the distributions. The objective of the statistical characterization undertaken in this work is to quantify a number of parameters that define the morphology and crystallography of a polycrystalline metal or alloy. In particular, a nickel-base superalloy is investigated in this work. In addition, the correlation between different parameters is studied and appropriate functions are developed. In the following section, the measurements of grain volume, number of contiguous neighbor grains and grain shape are described. These parameters have been selected to characterize the morphology of grains. The orientation distribution function (ODF), misorientation distribution function (MODF) and micro-texture function (MTF) are also calculated to describe the crystallography of the material.

4.1. Grain volume

As previously mentioned, each data point is considered to be a voxel in 3D space and thus has an associated volume given by $V_{\text{voxel}} = \delta\varepsilon^2$, where δ is the section thickness and ε is the step-size of the EBSD map. During the grain-identification process each voxel is assigned to a grain based on its misorientation with its neighbors, as defined in Eq. (1) [22,23]. The grain volume is given by $V_{\text{grain}} = N_{\text{v}} \cdot V_{\text{voxel}}$, where N_{v} is the number of voxels in the grain. Fig. 4 shows the distribution of grain volumes normalized by the mean volume. The mean grain volume is calculated to equal 37.32 μm^3 using:

$$\langle V_{\text{grain}} \rangle = \frac{\sum_{N_{\text{g}}} V_{\text{grain}}}{N_{\text{g}}} \tag{2}$$

where N_{g} is the number of grains. The largest grain had a value of $V_{\text{grain}}/\langle V_{\text{grain}} \rangle$ equal to 17.11. The distribution clearly is skewed with ~70% of the grains having less than the average grain volume.

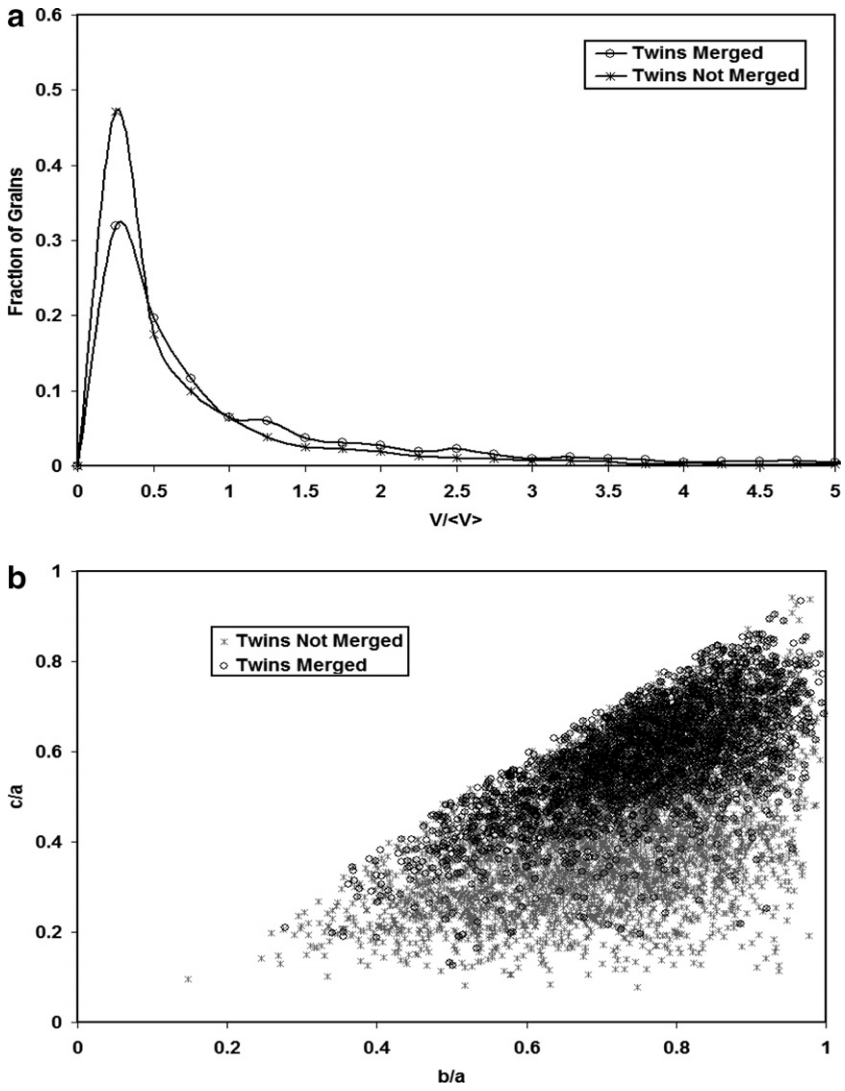

Fig. 3. Effect of merging twins with parent grains on: (a) normalized grain volume distribution, and (b) aspect ratios. Including the twins (i.e. not merging them) tended to shift the volume distribution towards smaller volumes. Also, the grains tended to become even more plate-like.

In addition to generating the true grain volume distribution, the distribution of equivalent sphere radii (ESR) is generated as

$$\mathrm{ESR} = \left(\frac{3}{4\pi} V_{\mathrm{grain}}\right)^{\frac{1}{3}} \tag{3}$$

where V_{grain} is the grain volume. The resulting distribution is also shown in Fig. 4. The distribution of grain ESR and its form have been investigated previously [19]. Enomoto [19] has compared various theoretical distributions to the experimentally measured grain ESR distribution for a polycrystalline iron sample in 3D. Feltham [27] has shown that the distribution of grain ESR tends to be log-normal, which is expressed as

$$f(R) = \frac{b}{\sqrt{\pi} R} \exp\left[-b^2 \left\{\ln\left(\frac{R}{R_{\mathrm{m}}}\right)\right\}^2\right] \tag{4}$$

where R_{m} is the median value in the log-normal distribution of $\mathrm{ESR}/\langle \mathrm{ESR} \rangle$ and was determined to be 0.91 for the IN100 dataset. The constant b for the dataset was calculated to be 1.68 by the least-squares method. The values of R_{m} and b for the IN100 dataset are similar to Enomoto's calculations for polycrystalline iron, where R_{m} was 0.98 and b was 1.63. Although it does appear that the $\mathrm{ESR}/\langle \mathrm{ESR} \rangle$ distribution for IN100 is slightly more log-normal than that for the iron sample of Enomoto. The curve representing the log-normal distribution in Fig. 4 appears to compare nicely with the experimental data over nearly all grain ESR. However, the log-normal distribution begins to over-predict the number of grains at large values of $\mathrm{ESR}/\langle \mathrm{ESR} \rangle$ (>3).

From grain growth theory, two alternate grain size distributions have been proposed and these have been compared to the present data. Hillert [28] has developed a function to define the grain size distribution by combining

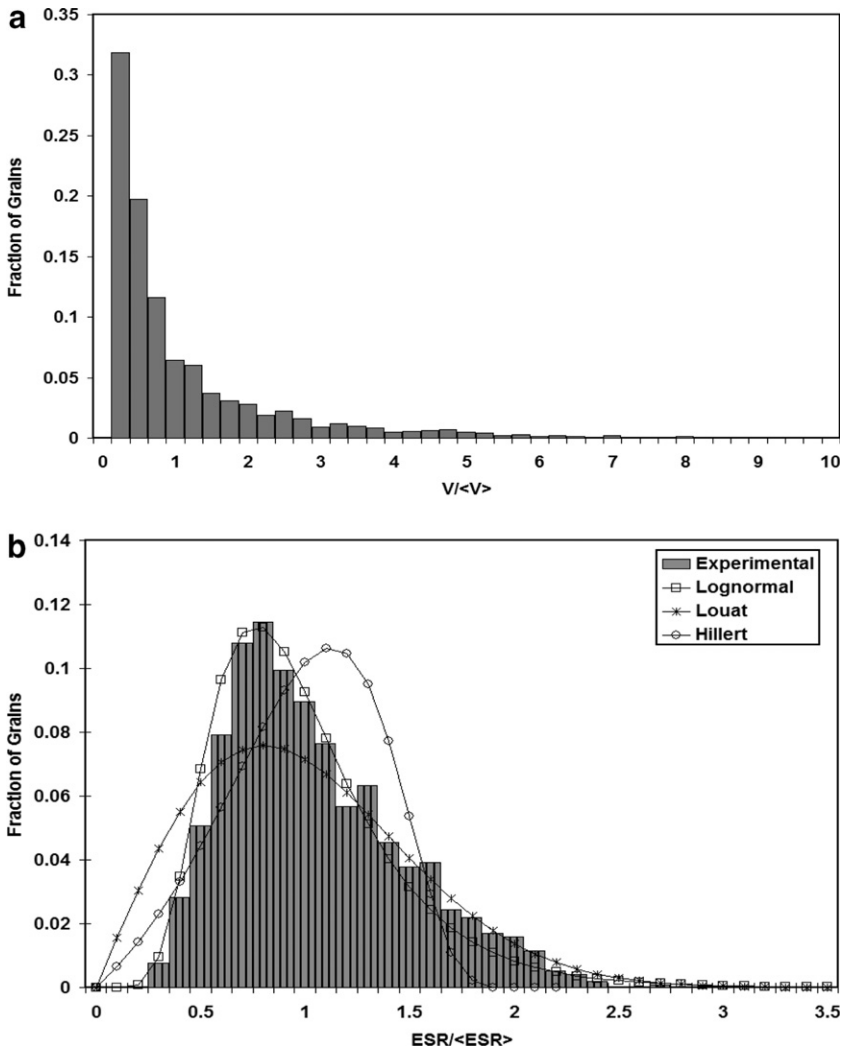

Fig. 4. (a) Distribution of grain volume for 2704 grains. $\langle V_{grain} \rangle = 37.32\ \mu m^3$. (b) Distribution of equivalent sphere radii. $\langle ESR \rangle = 1.76\ \mu m^3$. Curves representing the Hillert distribution, the Louat distribution and the log-normal distribution are overlaid on the experimental data and discussed in the text.

the theory of Ostwald ripening with grain growth. The function is:

$$f(u) = A\frac{u}{(2-u)^{2+\beta}}\exp\left(-\frac{2\beta}{2-u}\right) \tag{5}$$

where $u = R/R_{cr}$ and R_{cr} is given by $\langle R \rangle = 8R_{cr}/9$. In Eq. (5), A is a constant, determined by least-squares to be 43 for this dataset, and $\beta = 3$ for growth in 3D. The Hillert distribution is shown in Fig. 4 and significantly shifts the peak to a larger ESR than seen in the experimental data. However, the experimental dataset shows a noticeably longer tail resulting in a considerably larger maximum grain size than predicted from the Hillert model. Alternatively, Louat [29] focused on grain volume with the assumption that growth of boundaries is similar to a diffusion-like process. This theory [29] is common in the analysis of grain growth and gives the grain size distribution expressed by

$$f(R) = CR \cdot \exp(-\alpha R^2) \tag{6}$$

In Eq. (6), C and α are constants that are calculated by the least-squares method to be 0.158 and 0.78, respectively, for this dataset. The Louat distribution is also shown in Fig. 4 and appears to represent the larger grains nicely, but clearly overestimates the number of small grains.

While selected comparisons were made between the experimental and ideal grain-size distributions, the observed deviations from those ideal distributions may be the result of an inability to differentiate between the γ and γ' microconstituents and, from the presence of grain-boundary carbides in the alloy. As mentioned previously, the primary γ' microconstituent maintains a portion of semi-coherent interface with its parent grain, while its remaining interface is an incoherent grain boundary. Also, carbide particles are formed during the alloy processing and some of these ultimately reside on grain boundaries and affect grain growth. The presence of these phases and their attributes in the microstructure complicates the decision of which model to select and what fitting parameters are appropriate. Given that the primary γ' is semi-coherent

with the grains, the choice to merge these particles with their crystallographically similar parent grain is reasonable. However, the differences between the experimentally measured and theoretical distributions may ultimately offer insight into the interactions between the phases and their effects on the grain-growth process. The size distributions of the γ and γ' microconstituents need to be separated, compared individually and analyzed further to develop the understanding of poly-constituent grain growth, which is a topic for later investigation.

4.2. Number of contiguous neighbor grains

The number of contiguous neighbors per grain is one example of a parameter that cannot be determined directly from 2D measurements. Previous studies have characterized the quantity using different experimental methods. In Ref. [19], serial-sectioning has been used to examine a 3D volume, where each grain was followed through the sections and the number of grains that came in contact with it was recorded. In the present analysis, all voxels that neighbor the voxels of a given grain are located. The grain to which each neighboring voxel belongs is added to the list of grains that neighbor the current reference grain. Note that only voxels that share a common face, not a common edge or corner, with a voxel in the reference grain are considered. This requires the grains share some actual area and avoids counting grains that meet at only an edge or point. Fig. 5 shows the distribution of the number of contiguous neighbors for IN100. The mean number of contiguous neighbors $\langle N \rangle$ for the dataset is 12.9. The mean value for IN100 lies close to experimental observations for β-brass ($\langle N \rangle = 11.8$) [30], Al–Sn alloys ($\langle N \rangle = 12.48$) [31] and iron ($\langle N \rangle = 12.1$) [19]. However, the value deviates from the value of 14 associated with space-filling Kelvin polyhedra [32], and more significantly from random Voronoi polyhedra, where the mean number of contiguous neighbors has been shown to be 15.5 [33]. Krill and Chen [34] have investigated the mean number of contiguous neighbors for multiple structure generation techniques.

4.3. Grain shape and principal axes orientation

The irregular geometries that are typical of grains in a polycrystalline microstructure make grain shape a difficult parameter to quantify. This is especially true because of the lack of an ability to describe 3D shape in general [35]. Most descriptions of shape involve combining groups of size parameters to generate a unitless value [35]. Examples include: length/width (aspect ratio), area/convex area (solidity) and length/fiber length (curl). One common descriptor used to quantify grain size is the equivalent sphere radius (ESR), given previously by Eq. (5), regardless of the grain's true shape. This practice is useful to quantify grain volume, but does not offer much information about shape. Another common practice is to fit an ellipsoid (or ellipse in 2D) to the grain [8,9], which is the method selected for this work. A systematic method of generating ellipsoidal inclusions from voxel data obtained by serial-sectioning has been developed in Refs [36,37]. In the present work, the methods developed in [36,37] to generate geometric parameters of the ellipsoidal grain are used. In this method, the zeroth order moment (I_0), first-order moments (I_x, I_y, I_z) and second-order moments (I_{xx}, I_{yy}, I_{zz}) are first calculated for each grain by adding the contribution of each voxel belonging to an identified grain. The centroidal coordinates of the best-fit ellipsoid are next computed from the zeroth- and first-order moments as

$$x_c = \frac{I_x}{I_0}, \quad y_c = \frac{I_y}{I_0}, \quad z_c = \frac{I_z}{I_0} \tag{7}$$

Next, the principal directions, corresponding to the principal axes of the ellipsoid are calculated from the eigenvalues and eigenvectors of the second order moments

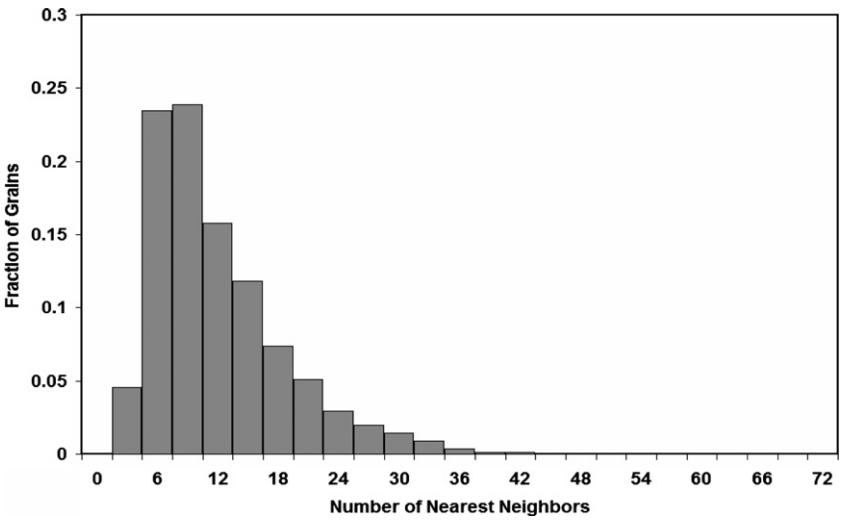

Fig. 5. Distribution of number of contiguous neighbors. The mean value of 12.9 neighbors is similar to experimental observations of other metallic alloys [19,28,29].

I_{ij}, i, $j = 1, 2, 3$. The major axis ($2a$), minor axis ($2c$) and intermediate axis ($2b$) of the ellipsoidal grain are solved from the relations of the principal second moments of inertia as

$$a = \left[\frac{A^4}{B \cdot C}\right]^{\frac{1}{10}}, \quad b = \left[\frac{B^4}{A \cdot C}\right]^{\frac{1}{10}}, \quad c = \left[\frac{C^4}{A \cdot B}\right]^{\frac{1}{10}} \tag{8}$$

where A, B and C are given by

$$A = \left(\frac{15}{4\pi}\right) \cdot \left(\frac{I_1 + I_2 - I_3}{2}\right),$$

$$B = \left(\frac{15}{4\pi}\right) \cdot \left(\frac{I_1 + I_3 - I_2}{2}\right), \quad C = \left(\frac{15}{4\pi}\right) \cdot \left(\frac{I_2 + I_3 - I_1}{2}\right)$$

Fig. 6 is a plot of the aspect ratios (b/a and c/a) for each grain. In Fig. 6, the upper right corner represents equiaxed grains; while the lower right and lower left corners represent a disk and needle, respectively. Many of the grains are seen to have a slightly elongated shape, but remain closest to the equiaxed corner of the plot. However, there are a significant number of grains that show a more pronounced deviation from equiaxed geometry. Fig. 6 shows the spatial distribution of the largest principal axis for each grain, identified as the shape orientation distribution. The direction, in the sample reference frame, is represented as the point where the vector in the direction of the largest principal axis intersects a unit sphere. The plot shows that there is no strong preferred shape orientation for the grains.

In some cases, the ellipsoidal representation of grains is an oversimplification that should be compensated. Correspondingly, an accuracy indicator in the ellipsoidal representation, termed as the relative ellipsoidal misfit, is used. The best-fit ellipsoid based on the moment analysis is scaled slightly to be of the same volume as the grain with the same aspect ratios and shape orientation. The fraction of the grain's voxels that lie within the best-fit ellipsoid is calculated. If the grain is perfectly ellipsoidal then the value of this quantity would be very near 1 (with the voxel size controlling the nearness to 1). Decreasing values of ellipsoidal misfit indicate more complex and likely concave shapes. Fig. 7 shows the distribution of the ellipsoidal misfit and also quantifies this as a function of grain size. Note that

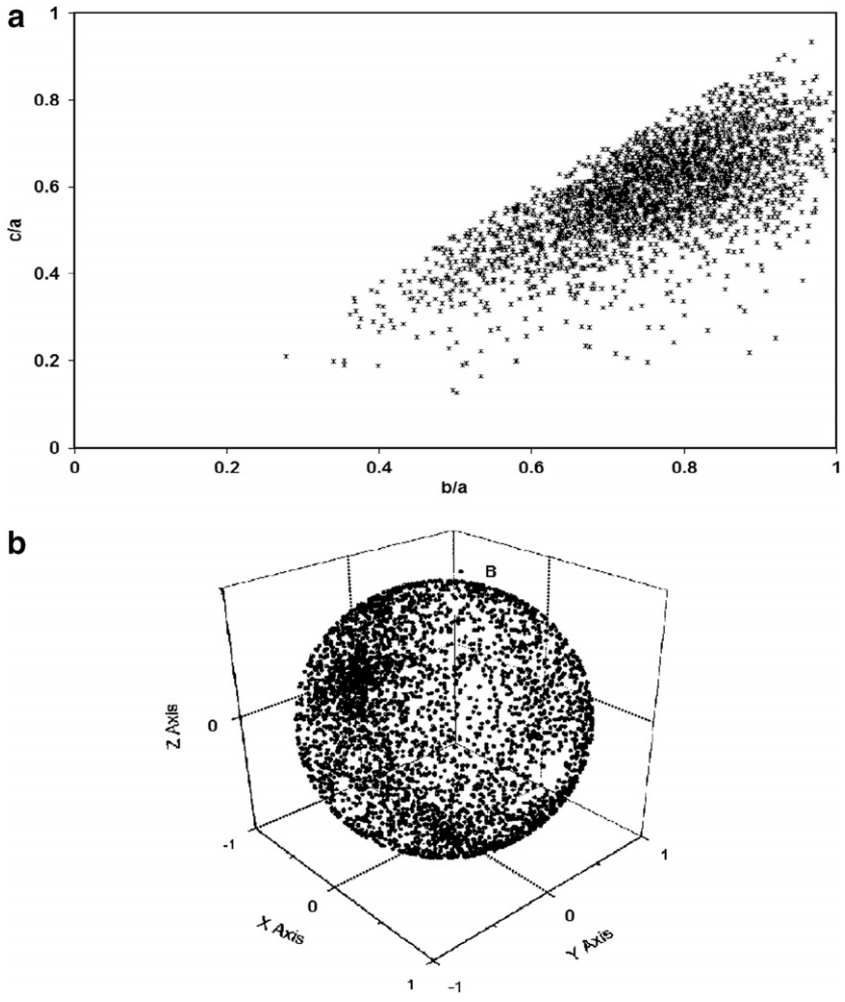

Fig. 6. (a) Plot of aspect ratios for each grain. The principal radii are such that $a > b > c$. The upper right corner represents a sphere, while the lower right and lower left represent a disk and needle, respectively. (b) Orientation of the largest principal axis relative to the sample coordinates. The points correspond to the intersection of the principal axis vector with a unit sphere. There appears to be no preferred shape orientation.

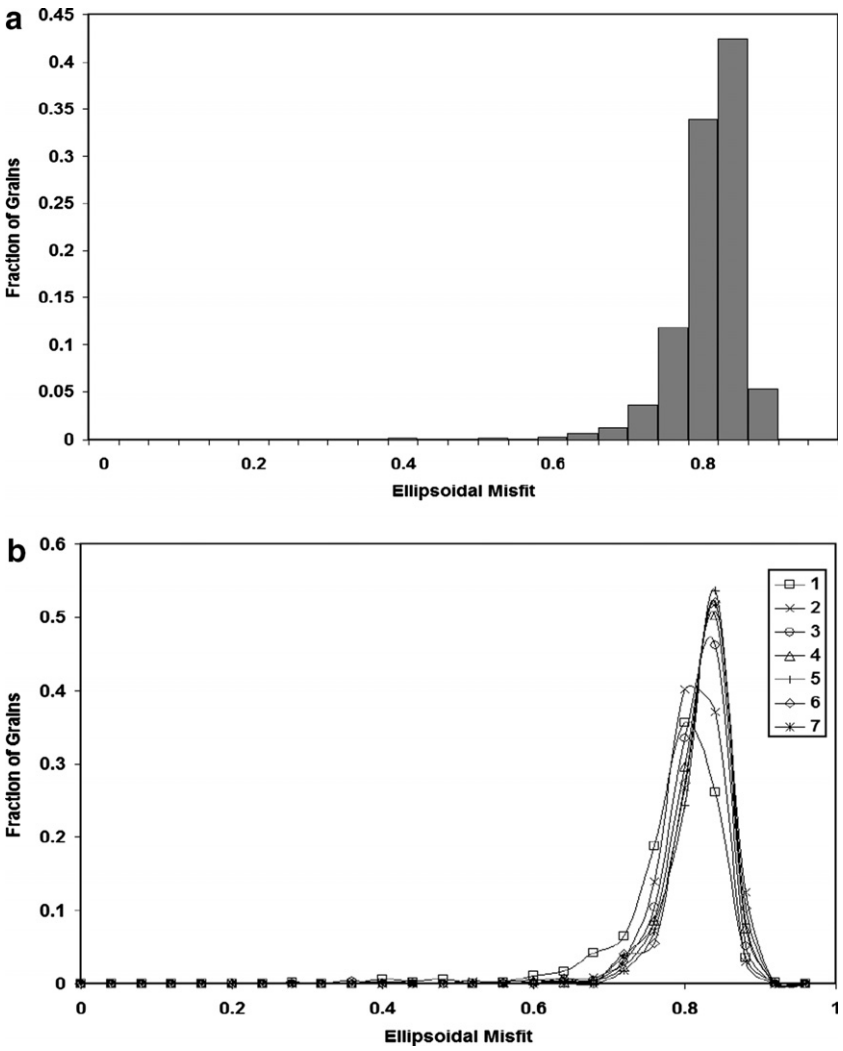

Fig. 7. (a) Distribution of ellipsoidal misfit of the best-fit ellipsoid. A value of 1 implies a perfect ellipsoidal grain, while decreasing values imply more complicated and likely concave shapes. (b) Distribution of ellipsoidal misfit for varying sizes. The values drop suddenly at small grain sizes. This is likely the result from errors in the moment calculations introduced by the limited number of voxels sampled for the small grains.

the ellipsoidal misfit becomes worse as the grain size decreases. One plausible explanation for this is that the small number of voxels in the small grains can affect the moment calculations used to generate the best-fit ellipsoid. In general, the values of ellipsoidal misfit are relatively high, which indicates that the ellipsoid representation is relatively accurate for most grains.

4.4. Surface area

The calculation of surface area using the current set of voxel data is complicated by the fact the discrete voxels produce excess surface area. For the voxel representation, the exact surface area of the grains can be determined by the number of voxel faces on the grain boundary. However, this value is expected to be significantly higher than the actual surface area, because of aliasing effects. Another method for quantifying surface area of the voxelized data is to consider the fraction of voxels that lie on the surface of the grain. This quantity actually measures the surface-to-volume ratio. The major complication with this measurement is the significant effect that the voxel resolution has on the value. As the voxel size increases, the fraction of voxels on the surface of the grain rapidly increases towards 1. However, if the voxel dimensions are quite small compared to the grain size, then the value gives an accurate measure of surface-to-volume ratio. Fig. 8 shows the distribution of fraction of surface voxels. Many of the grains are seen to approach a value of 1 due to the poor resolution relative to their size. As will be shown later, nearly all of the grains with a value near 1 are of extremely small size.

4.5. Crystallography

The previous parameters provided information about the morphological nature of the grains, but their crystallo-

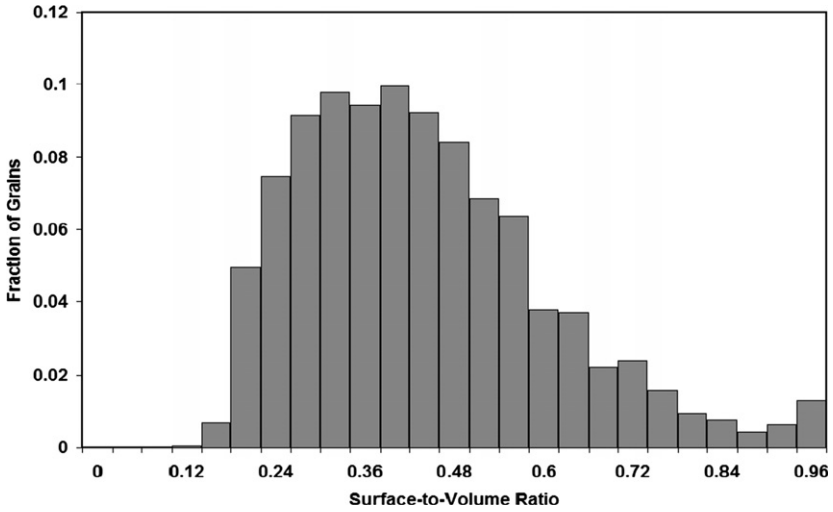

Fig. 8. Distribution of surface-to-volume ratio, which is simply the fraction of a grain's voxels on the surface of the grain. Small values imply larger and/or more spherical grains. Resolution greatly affects smaller grains resulting in many values approaching 1.

graphic nature was not examined. This section presents three parameters used to describe the crystallography of the grains.

4.5.1. Orientation distribution function (ODF)

The orientation distribution function (ODF) is a measure of the macroscopic texture of a material. The crystallographic orientation of each grain is plotted on a stereographic projection for a particular crystallographic direction, and the presence of any preferred orientations becomes evident [38]. Macroscopic textures are common in heavily worked samples and recrystallized samples [39–41]. Fig. 9 shows the pole figures for the experimental volume, having an angular accuracy of $\pm 1°$. Note that the number of grains in the volume is in the range of that typically used to produce an ODF [42]. All of the sampled grains were used in this plot because intersection with the edge of the volume only effects morphological measurements, not crystallographic ones. Clearly, from Fig. 9 there is no noticeable macroscopic texture in this material. There is little clustering in any of the pole figures, with the only apparent higher polar density regions being an artifact of the projection process, which makes poles near the center appear more clustered.

4.5.2. Misorientation distribution function (MoDF)

The MoDF provides information on the local arrangement of grains. Misorientation is the relative change in orientation from one grain to another, usually a neighboring grain, and is often referred to as the orientation difference. When reporting misorientation, a common practice is to report the smallest angular rotation necessary to rotate one orientation onto another [38]. Small misorientation angles correspond to grains of similar orientation. Fig. 10 shows the distribution of misorientation angles. The MoDF for this material shows that neighboring grains are likely to have a large misorientation, as is evident from few low angle misorientations in the MoDF. In fact, the distribution has similar shape to that derived by MacKenzie [43] for randomly oriented cubes.

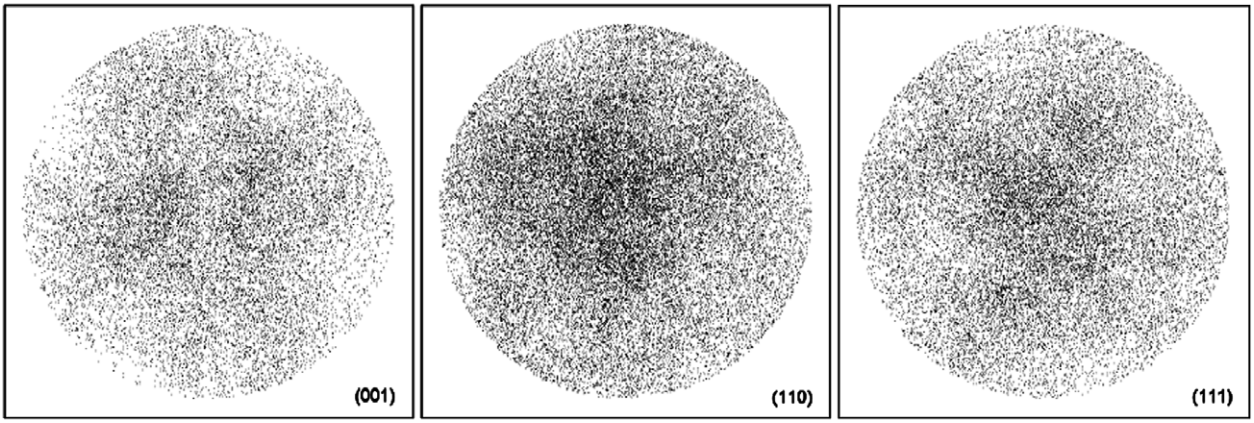

Fig. 9. Pole figures for 4373 grain orientations.

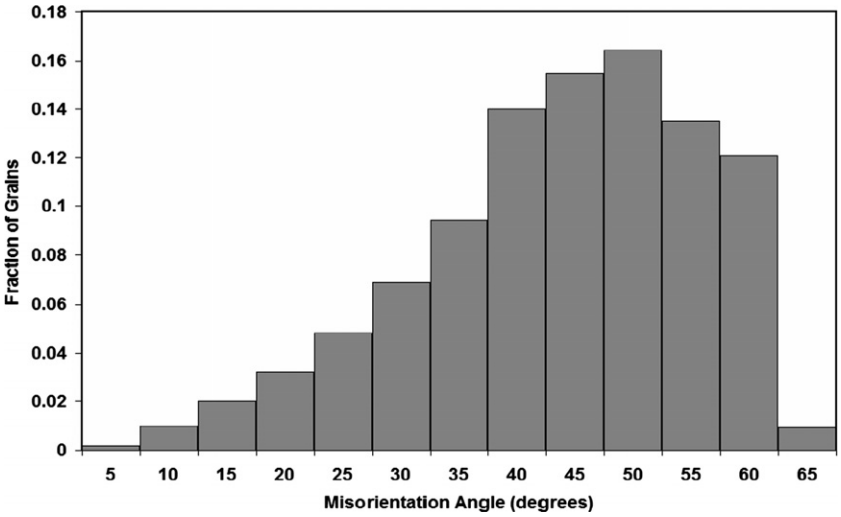

Fig. 10. Distribution of misorientation angles.

4.5.3. Micro-texture function (MTF)

The MTF is a measure of the amount of clustering of orientations and misorientations [44]. It is similar in nature to the MoDF, but gives information on a more local level. The MoDF gives the number of misorientations in the entire structure while the MTF describes how the lowest misorientations are spatially arranged relative to a given grain. The MTF is a distribution of the fraction of contiguous neighbor grains having "low misorientation". In this work, 15° was selected as the cutoff for considering a misorientation to be low. In determining the MTF, the misorientation between a grain and each of its neighbors is calculated. Then, the fraction of those misorientations below 15° is determined. Fig. 11 shows the distribution of the fractional values. A high fraction implies that locally a large number of similarly oriented grains are clustered together. As previously mentioned, the MoDF showed a small number of low angle misorientations in this material. As a result, it is not expected that many grains would have a high fraction of neighbors with low misorientation. This expectation is confirmed by the MTF, which shows that no grains share low angle misorientations with more than half their neighbors. There have been studies [44] involving materials that show significant micro-texture. Approximately 5% of the grains in a Ti-6242 sample in Ref. [44] had low-angle misorientations with at least two-thirds of their neighbors.

5. Parameter correlations

The correlation or mutual relationship between geometric parameters described in the previous section is important because it provides additional information regarding the morphology and spatial arrangement of grains. The

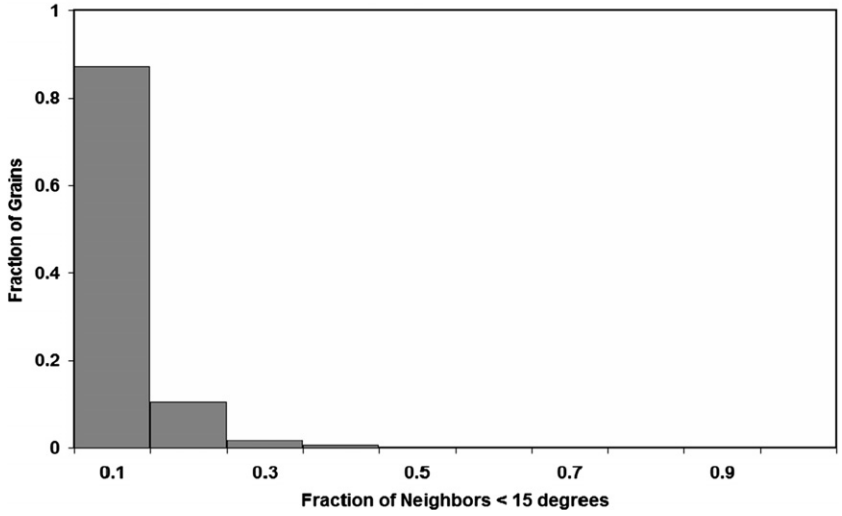

Fig. 11. Micro-texture function (MTF) quantifying similar orientation clustering. A high fraction corresponds to a grain having most of its neighbors similarly oriented. In this material there is no significant local texture since no grains have many similarly oriented neighbors.

correlations investigated in this work are all specified to have volume as the independent parameter, and the change in other parameters are studied as a function of volume. Note that the volume of each grain was converted into an equivalent sphere radius (ESR) using Eq. (5) to simplify delineating ranges of grain volume. Grains are placed in their appropriate equivalent sphere diameter (2 ESR) bin and the distributions of each parameter were generated and compared across the diameter bins. For each diameter bin, representing a range of grain volumes, Table 1 lists the average value of each parameter. Note that the 1 μm diameter bin contains grains with diameter between 1 and 2 μm, the two diameter bin contains grains with diameter between 2 and 3 μm and so on.

Plots of these relationships are shown in the following subsections, but it is also desirable to quantify the degree of correlation between two selected parameters. To accomplish this goal, a quantity called the correlation ratio, η^2, is used [45]. The correlation ratio is a preferred metric in comparison to the correlation coefficient, r, because it can be used with non-linear relationships. The correlation ratio is the square of the correlation coefficient (r^2) if the relationship is linear. If the relationship is non-linear, the magnitude of the correlation ratio is larger, but retains a value between 0 and 1. The formula for the correlation ratio is given by

$$\eta^2 = \frac{\sum_{b=0}^{N_b} n_b (\bar{y}_b - \bar{y})^2}{\sum_{i=0}^{N_g} (y_i - \bar{y})^2} \tag{9}$$

where N_g is the total number of grains, N_b is the number of bins, n_b is the number of observations in a given bin b and

$$\bar{y}_b = \frac{\sum_{i=0}^{n_b} y_{bi}}{n_b}, \quad \bar{y} = \frac{\sum_{b=0}^{N_b} n_b \bar{y}_b}{\sum_{b=0}^{N_b} n_b}$$

The correlation ratio can be thought of as the percentage of the total variance of the dependent variable accounted for by the variance between groups of the independent variable. Equation 9 shows that if there is a large difference between the mean of the whole data set and the means of the individual bins, then the correlation ratio is high. The degree of correlation can be generalized into three groups: small (0–0.3), medium (0.3–0.5) and large (0.5–1) [45]. The correlation ratios of the relationships will be presented in the following subsections.

5.1. Correlation of number of contiguous neighbors as a function of grain diameter

The number of contiguous neighbors as a function of grain size was studied in Ref. [19] for iron which matched well with experiments using aluminum in [46]. Additionally, it is known from the perimeter law that the number of edges (or neighbors) of a 2D grain is proportional to its radius [19]. Studying this relationship in 3D may yield a similar law for 3D grains. Fig. 12 shows the distributions of number of neighbors as a function of grain diameter. Clear from the figure is that the average number of neighbors increases with grain size. This agrees with previous studies by Enomoto [19], although number of neighbors was considered as the independent variable in that work. The trend of the curves in Fig. 12 is simply the reverse of that in [19]. The correlation ratio for number of neighbors and grain diameter has been calculated as 0.84. This high value confirms the visual evidence of a strong correlation between the two parameters.

5.2. Correlation of diameter of neighboring grains with reference grain diameter

The number of contiguous neighbors offers information about the number of grains contacting a reference grain, but yields no information on the size distribution of the neighbors. The spatial arrangement of grains can be better understood if the size of grains that neighbor each other can be quantified. Fig. 13 shows the distribution of neighboring equivalent sphere diameters as a function of the diameter of the reference grain. For this material, the distribution of the size of the neighboring grains is not strongly dependent on the reference grain's size. There appears to be a minimal shift towards slightly larger neighbors for small grains, but not a dramatic difference from larger grains. The very low correlation ratio of 0.001 confirms this assessment.

Table 1
Average values of selected parameters as a function of equivalent sphere diameter

Diameter or 2 ESR (μm)	Number of grains	Number of neighbors	Average neighbor diameter or 2 ESR (μm)	*b*/*a*	*c*/*a*	Surface-to-volume ratio	Ellipsoidal misfit
1	356	6.51	4.49	0.75	0.55	0.75	0.80
2	832	8.75	4.49	0.76	0.58	0.54	0.82
3	639	12.11	4.46	0.75	0.58	0.41	0.83
4	394	16.24	4.39	0.75	0.59	0.33	0.84
5	259	20.23	4.39	0.77	0.60	0.28	0.84
6	146	25.67	4.33	0.76	0.60	0.24	0.84
7	56	30.79	4.30	0.78	0.62	0.21	0.85

Each grain's volume is converted into an equivalent sphere diameter using Eq. (5) and each grain is then placed in the corresponding bin.

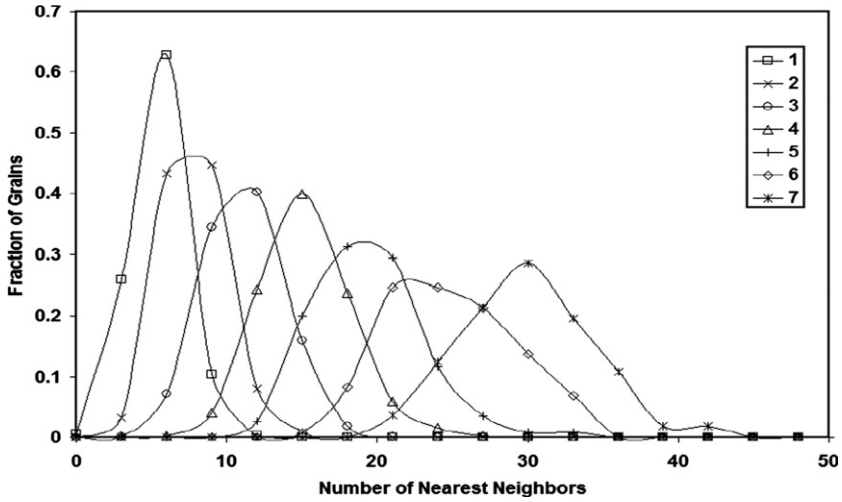

Fig. 12. Distribution of number of contiguous neighbors for grains of varying size. Increasing number of neighbors with increasing size matches previous observations [19]. The parameters are clearly correlated by the noticeable shift, and the value of $\eta^2 = 0.84$ determined for the data.

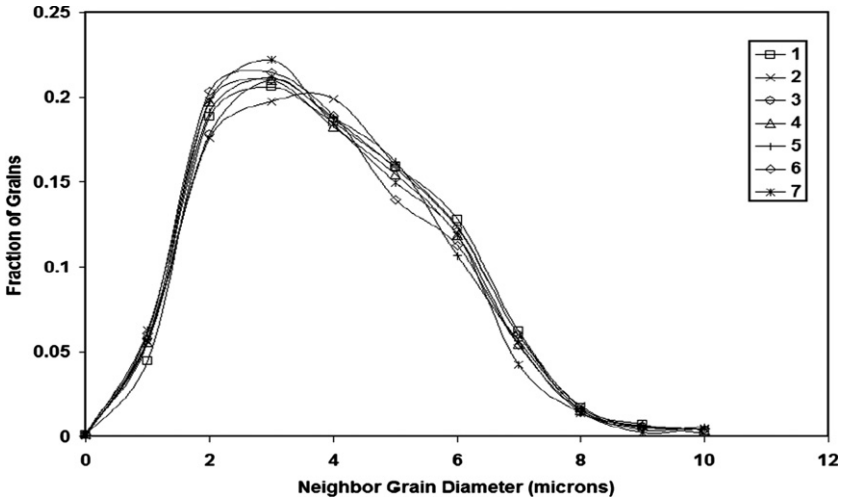

Fig. 13. Distribution of neighboring grain diameters for grains of varying diameter. There is no correlation with varying grain diameter, since the distributions remain similar over all different sizes.

5.3. Correlation of grain shape as a function of grain diameter

In the current analysis, the aspect ratios of the best-fit ellipsoid are studied as a function of grain diameter. In order to fully define the ellipsoid, two aspect ratios are needed. Ideally, one would want to measure the correlation between size and shape by determining the aspect ratio b/a as a function of grain diameter, and then also correlate the aspect ratio c/a as a function of b/a for each size bin. However, while the number of grains is generally sufficient to describe the first aspect ratio distribution relative to grain diameter, the number of grains was too few (i.e. $<$50 grains/bin) to describe the second aspect ratio's distribution. As a result, we have related the two aspect ratios to grain diameter individually, as shown in Fig. 14. The correlation ratios for each parameter are extremely low; 0.009 and 0.02 for b/a and c/a, respectively, i.e. grain shape does not correlate strongly with grain size. The values of c/a for the smallest grains (diameter bins 1 and 2) slightly extend lower than those of the medium and larger grains. This is likely the result of the fact that the smaller grains are more significantly affected by resolution. During calculation of a grain's moments (Section 4.3) each voxel is used as a discrete point. The fewer the number of voxels in a grain, the larger the contribution each voxel has on the moment calculation. A couple of voxels added (or subtracted) from a small grain can significantly alter the measured aspect ratios. The addition or subtraction of voxels from a grain could result from the selected data resolution resulting in more or fewer points within a feature of a given size, or it could be due to the grain assignment of problematic data during data clean-up. If a voxel near the boundary were either assigned or not assigned to a particular grain, the effect would be felt much more for a small grain. The following section will discuss the metric chosen in this

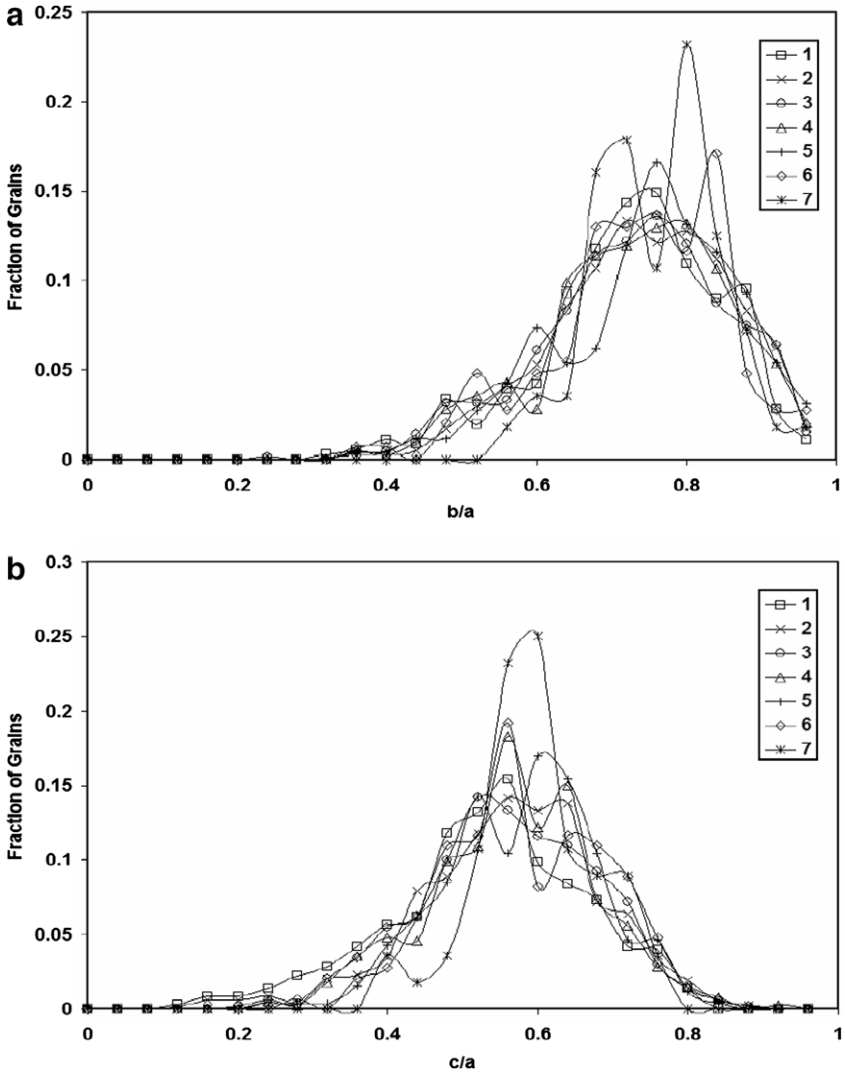

Fig. 14. Distribution of (a) b/a and (b) c/a for grains of varying diameter. There appears to be no significant correlation between the aspect ratios and the grain size. There is a shift to smaller aspect ratios for c/a than b/a, which is due to the definition of $a > b > c$. Additionally, the small deviation of the c/a values for the smallest grains has been attributed to inadequate voxel resolution.

work to quantify resolution relative to the size of individual grains and will offer some insight into the resolution necessary for accurate description of grain shape.

5.4. Correlation of surface-to-volume ratio as a function of grain diameter

Surface-to-volume ratio is the final parameter to be correlated to grain diameter. As previously discussed, the method for determining surface area-per-volume is highly dependent on the voxel dimensions relative to the grain size. As a result, the grains in the large size bins can be considered accurate, but the grains in the smaller size bins may have erroneously high surface-to-volume-ratio values. Fig. 15 shows the change in surface-to-volume ratio with change in grain size. The trend of increasing surface area-per-volume with decreasing grain size is clear and agrees with expectations. However, the rate of increase is likely smaller than seen in Fig. 15, when considering the effect of relative resolution in the smaller size bins. Surface-to-volume ratio and grain diameter showed the largest amount of correlation with a correlation ratio of 0.86. Seen in Fig. 15, the grains in the 1 μm diameter bin have very poor relative resolution and the majority have at least 70% of their voxels on the surface of the grain. This finding tends to support the general rule mentioned earlier for the need of at least 10 sections through a feature for proper reconstruction and characterization. A discretized sphere with 10 voxels across its diameter would yield a surface-to-volume ratio of ~0.50. The two smallest grain size bins (1 and 2 μm diameter) are below that threshold and these show the most deviation in all the correlation plots. The combination of Figs. 14 and 15 provide some evidence that accurate description of shape requires, at minimum, ~50% of voxels be contained within the bulk of a grain or feature. This minimum value realistically only provides the ability

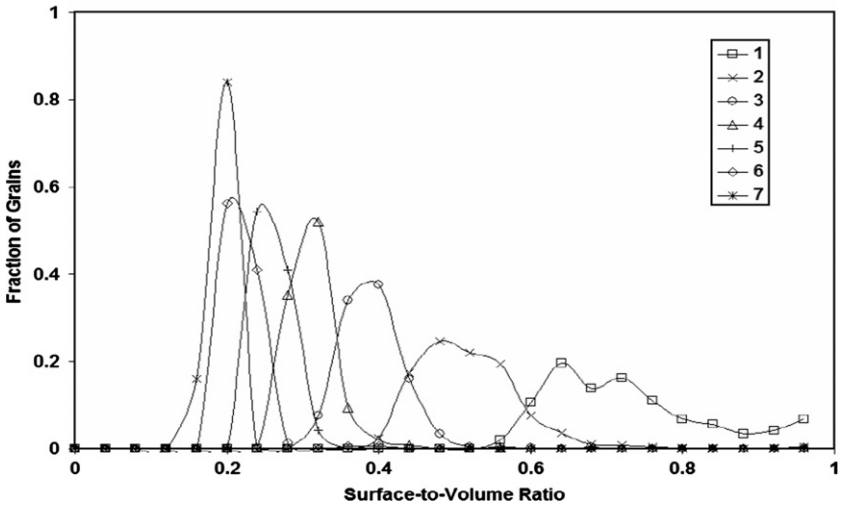

Fig. 15. Distribution of surface-to-volume ratio for grains of varying diameter. There is strong correlation since the distribution shifts dramatically over the different sizes. The rate of shift to higher fractions as diameter decreases is likely accelerated by poor relative resolution in the smaller grains. The smallest grain size bin shows very poor relative resolution considering the extremely high fraction of voxels on the grain surface.

to quantify general descriptions of shape (i.e. aspect ratios). Quantification of local boundary curvatures likely requires a much higher data resolution relative to the feature sizes.

6. Conclusions

This study outlines a method for unbiased materials characterization in three dimensions. The distributions of morphological parameters such as: grain volume, number of contiguous neighbors, aspect ratio and surface-to-volume ratio, are calculated for 2704 fully contained grains. Crystallographic parameters such as: the ODF, the MoDF and the MTF are also calculated. In addition to the individual distributions, the correlation between each parameter and grain size is investigated. The grain size distribution is seen to follow a lognormal distribution and varies noticeably from some selected alternate distributions. However, the observed deviation from these ideal distributions may be attributed, in part, to an inability to distinguish between the γ and γ' phases in the alloy. The average number of neighbors was found to be 12.9, which is similar to previous results for a number of different metallic alloys [19,30,31]. The average number of neighbors is seen to deviate more significantly from values obtained for space filling polyhedra [32,33]. Some grains were seen to be nearly equiaxed, but in most cases the grains show elongation or flattening. The number of neighbors and surface-to-volume ratio are seen to be highly correlated to grain size, but neighboring grain size and shape show no significant correlation to grain size. The misorientation distribution function (MoDF) is seen to be similar to the random distribution derived by MacKenzie [43]. The micro-texture function (MTF) is found to contain no grains with many similarly oriented neighbors, agreeing with the MoDF.

This first part of two-part description shows a step-wise advance in the field of quantitative 3D microstructure (grain structure) characterization. The amount of quantitative information available in the collected dataset surpasses that commonly available through 2D stereological methods and is invaluable for representing grain structures in modeling. Additionally, the tools created to analyze the 3D data are an important development in the automation of the 3D characterization process. The second of this two-part paper will focus on direct application of this characterization technique and the resulting distribution and correlation functions in the generation of statistically equivalent synthetic 3D grain structures.

Acknowlegement

The authors acknowledge support from the Materials and Manufacturing Directorate and the Air Force Office of Scientific Research. MAG and SG acknowledge support through contract # F33615-01-2-5225. Specifically, the authors would like to thank Craig Hartley for his advice and constant championing of this research.

The authors would also like to thank the members of the Microstructural Characterization Facility at AFRL/ML for their assistance.

References

[1] Uchic MD. JOM 2006;58(12):24.
[2] Spanos G. Scripta Mater 2006;55:3–5.
[3] Dimiduk DM, Parathasarathy TA, Rao SI, Choi YS, Uchic MD. In: Numiform 8 proceedings; 2004. p. 1705–10.
[4] Rhines FN, Craig KR, Rousse DA. Metall Trans A 1976;7A:1729–34.
[5] Barton NR, Dawson PR. Model Simul Mater Sci Eng 2001;9:433–63.
[6] Coster M, Arnould X, Chermant JL, El Moataz A, Chartier T. Image Anal Stereol 2005;24:105–16.
[7] Ballani F, Daley DJ, Stoyan D. Comp Mater Sci 2006;35:399–407.
[8] Saylor DM, Fridy J, El-Dasher BS, Jung KY, Rollett AD. Metall Trans A 2004;35A:1969–79.

[9] Brahme A, Alvi MH, Saylor D, Fridy J, Rollett AD. Scripta Mater 2006;55:75–80.
[10] Lewis AC, Geltmacher AB. Scripta Mater 2006;55:81–5.
[11] DeHoff RT. J Microsc 1983;131:259–63.
[12] Uchic MD, Groeber MA, Dimiduk DM, Simmons JP. Scripta Mater 2006;55:23–8.
[13] Zaafarani N, Raabe D, Singh RN, Roters F, Zaefferer S. Acta Mater 2006;54:1863–76.
[14] Groeber MA, Haley BK, Uchic MD, Dimiduk DM, Ghosh S. Mater Charact 2006;57:259–73.
[15] Williams R, Bhattacharyya D, Viswanathan GB, Banerjee R, Fraser HL. Proc Microsc Microanal 2004;10:1178–9.
[16] Desch CH. J Inst Met 1919;22:241–63.
[17] Dobrich KM, Rau C, Krill CE. Metall Trans A 2004;35A:1953–61.
[18] Lauridsen EM, Schmidt S, Nielsen SF, Margulies L, Poulsen HF, Juul Jensen D. Scripta Mater 2006;55:51–6.
[19] Zhang C, Suzuki A, Ishimaru T, Enomoto M. Metall Trans A 2004;35A:1927–32.
[20] Rowenhorst DJ, Gupta A, Feng CR, Spanos G. Scripta Mater 2006;55:11–6.
[21] Lewis AC, Bingert JF, Rowenhorst DJ, Gupta A, Geltmacher AB, Spanos G. Mater Sci Eng A 2006;418:11–8.
[22] Ghosh S, Bhandari Y, Groeber M. CAD 2007. doi:10.1016/j.cad.2007.11.003.
[23] Bhandari Y, Sarkar S, Groeber M, Uchic M, Dimiduk D, Ghosh S. Comp Mater Sci 2007;41:222–35.
[24] Xie CL, Ghosh S, Groeber M. J Eng Mater Tech 2004;126:339–52.
[25] Gunderson HJG. J Microsc 1977;111:219.
[26] DeHoff RT, Aigeltinger EH, Craig KR. J Microsc 1972;95:69–91.
[27] Feltham P. Acta Metall 1957;5:97–105.
[28] Hillert M. Acta Metall 1965;13:227–83.
[29] Louat NP. Acta Metall 1974;22:721–4.
[30] Hull FC. Mater Sci Technol 1988;4:778–85.
[31] Williams WM, Smith CS. Trans AIME 1952;194:755–65.
[32] Thompson (Lord Kelvin) W. Philos Mag 1887;24:53.
[33] Wakai F, Enomoto N, Ogawa H. Acta Mater 2000;48:1297–311.
[34] Krill CE, Chen LQ. Acta Mater 2002;50:3057–73.
[35] Russ JC. The image processing handbook. third ed. CRC Press; 1998. pp. 512–515.
[36] Li M, Ghosh S, Richmond O, Weiland H, Rouns TN. Mater Sci Eng A 1999;A265:153–73.
[37] Li M, Ghosh S, Richmond O, Weiland H, Rouns TN. Mater Sci Eng A 1999;A266:221–40.
[38] Cullity BD, Stock SR, Stock S. Elements of X-ray diffraction, third ed.; 2001.
[39] Miraglia M, Dawson PR, Leffers T. Acta Mater 2007;3:799–812.
[40] Ghosh Chowdhury S, Datta S, Ravi Kumar B, De PK, Ghosh RN. Mater Sci Eng A 2007;443:114–9.
[41] Glavicic MG, Semiatin SL. Acta Mater 2006;54:5337–47.
[42] Humphreys FJ. J Microsc 1999;195:170–85.
[43] MacKenzie JK. Biometrika 1958;45:229.
[44] Deka D, Joseph DS, Ghosh S, Mills MJ. Metall Trans A 2006;37A:1371–88.
[45] Kenney JF, Keeping ES. Mathematics of statistics. second ed. Van Nostrand; 1947. pp. 198–202.
[46] Rhines FR, Patterson BR. Metall Trans A 1982;13A:985–93.